Assessment of Land Subsidence Risk Changes in Agricultural Lands Using Remote Sensing Data (Golestan Province)

Fateme Garshasbi[1], Qadir Ashournejad[2*], Taher Safarrad[3]

[1]Dept of Geography and Urban Planning, Faculty of Humanities and Social Sciences, University of Mazandaran, Babolsar, Iran, f.garshabi05@umail.umz.ac.ir
[2]Dept of Geography and Urban Planning, Faculty of Humanities and Social Sciences, University of Mazandaran, Babolsar, Iran, ashournejad@umz.ac.ir
[3]Dept of Geography and Urban Planning, Faculty of Humanities and Social Sciences, University of Mazandaran, Babolsar, Iran, t.safarrad@umz.ac.ir

Keywords: Land subsidence, Agriculture, Subsidence risk, Remote Sensing, Golestan

Abstract

Land subsidence is one of the most significant environmental threats in agricultural areas, directly affecting soil stability and crop productivity. This study assessed changes in land subsidence in the agricultural lands of Golestan Province between 2015 and 2023. Sentinel-1 radar data were processed using the SBAS method and interferometry techniques to extract vertical ground displacements, while environmental and agricultural indicators, including NDVI, SMI, slope, and aspect, were integrated to analyze subsidence risk. The results indicated a substantial increase in both the intensity and extent of subsidence in 2023, with the average risk rising from 0.397 in 2015 to 0.750 in 2023, while risk dispersion decreased, leaving nearly all agricultural areas at high risk. Correlation analysis also revealed that agricultural activities play a significant role in accelerating subsidence (correlation coefficient = 0.71). Pixel frequency analysis and distribution charts further indicated spatial expansion of risk and homogenization of high-risk areas. These findings can inform sustainable agricultural land management and help predict areas prone to subsidence.

1. Introduction

Land subsidence, defined as the gradual or sudden sinking of the ground surface, results from both natural and anthropogenic processes and is particularly significant in agricultural areas due to intensive land use and changes in soil properties (Ashraf et al., 2024). Subsidence in agricultural lands is critical because it can adversely affect crop productivity, soil quality, and the economic sustainability of farmers. This phenomenon leads to soil compaction and cracking, alters water infiltration, restricts root growth, and reduces nutrient availability, ultimately diminishing crop yield and soil productivity (Merem et al., 2019). Moreover, land subsidence can disrupt irrigation infrastructure and increase the risk of flooding and other agriculture-related damages, posing a threat to rural livelihoods and food security in vulnerable regions (A.A et al., 2024). Despite its importance, policymakers often face challenges in identifying high-risk areas due to a lack of accurate spatial data. In this context, remote sensing and GIS technologies provide effective tools for spatiotemporal monitoring of land dynamics, offering valuable means for analyzing and managing subsidence risk (Ashournejad & Garshasbi, 2024). Previous studies have also highlighted the impact of land subsidence on agriculture. For instance, Lechner et al. (2016), using ALOS PALSAR imagery, demonstrated that subsidence alters soil physical properties such as compaction, cracking, and water permeability, leading to reduced field uniformity, decreased crop yields, and increased difficulty in agricultural operations. Sidiq Sidiq et al. (2019) reported that land subsidence also occurs in agricultural areas in Bandung, Indonesia, with a rate of approximately 5 cm per year during 2007–2011, as determined using ALOS PALSAR imagery and the SBAS method, emphasizing the importance of monitoring this phenomenon in farmlands. Xiao et al. (2021), through analysis of agricultural indices including biomass, leaf area index (LAI), soil moisture, and soil organic matter, investigated the relationship between subsidence and soil quality and productivity. Their results indicated that land subsidence can create waterlogged areas and reduce crop performance. Furthermore, Assadi et al. (2024) showed that cropping patterns and agricultural practices play a significant role in subsidence. In the Nourabad plain, rice fields experienced greater subsidence compared to wheat fields, based on Sentinel-1 and Sentinel-2 imagery. Despite numerous studies, the assessment of subsidence risk in agricultural lands of Golestan Province has not yet been conducted. This province, characterized by high geographical diversity and extensive agriculture—including wheat, rice, vegetables, and orchards—is one of the major production hubs in northeastern Iran. However, irrigation pressure and overexploitation of groundwater resources can threaten soil stability (Danhassan et al., 2024). Recent studies have also confirmed the concentration of subsidence in agricultural lands and its overlap with intensively cultivated areas (Ashraf et al., 2024). Therefore, the main objective of this study is to evaluate changes in subsidence risk in Golestan's agricultural lands over the period 2015–2023. In this context, slope, aspect, soil moisture, and vegetation cover (NDVI) were employed to analyze the relationship between the physical and biological characteristics of agricultural lands and the intensity of subsidence. These indicators were selected as representatives of moisture status, vegetation density, and topography, as their variations may reflect irrigation pressure, cropping patterns, and overexploitation of agricultural lands—key factors exacerbating

* Corresponding author

This contribution has been peer-reviewed. The double-blind peer-review was conducted on the basis of the full paper.
https://doi.org/10.5194/isprs-annals-X-4-W8-2025-257-2026 | © Author(s) 2026. CC BY 4.0 License.

subsidence. Finally, by comparing risk maps for 2015 and 2023, trends in subsidence were identified, providing a scientific basis for sustainable management of agricultural lands and mitigation of subsidence impacts.

2. Materials and methods

1.1 Study area

Golestan Province is located between 53°51′ and 56°01′ E longitude and 36°04′ and 38°07′ N latitude (Figure 1). The province's highest elevation reaches 3,813 meters, while the mean elevation is 230 meters and the lowest point is 20 meters below sea level. The annual precipitation averages approximately 450 mm, and the mean annual temperature typically ranges between 17.9 and 18.5 °C (Namazi Rad et al., 2021).

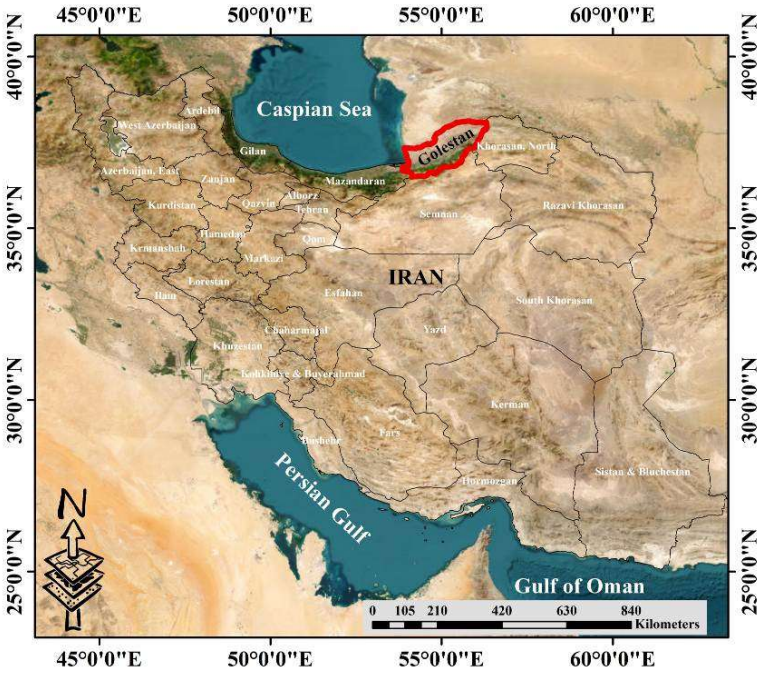

Figure 1. Map of the study area

1.2 Methods

1.2.1 Data processing

To investigate land subsidence in Golestan Province, radar data from Sentinel-1 equipped with a C-band Synthetic Aperture Radar (SAR) were used, providing continuous surface imaging under all weather conditions. Single Look Complex (SLC) Sentinel-1 data enabled the application of Interferometric SAR (InSAR) for measuring subtle ground deformations. The Interferometric Wide Swath (IW) mode was selected to achieve wide-area coverage with adequate spatial resolution. The dataset covered the period from 2015 to 2023 and formed the basis for generating subsidence maps. All InSAR processing steps were carried out directly from the original Sentinel-1 SLC data to produce deformation maps. To manage the large volume of Sentinel-1 data, Python libraries including Sentinelsat along with netrc configuration files were used to automate data access and organize SLC images systematically by year and time interval. In total, 192 images were collected, comprising temporal pairs with 6-, 12-, and 24-day intervals, enabling the analysis of both short-term variations and gradual subsidence trends. To generate interferograms, Master and Slave images were precisely co-registered to remove geometric, orbital, and topographic effects, ensuring accurate extraction of actual ground deformation. The co-registration was performed using a pixel-wise cross-correlation algorithm, achieving sub-pixel accuracy. The phase difference between the Master and Slave images was then calculated to quantify ground displacement over the study period. Each SLC pixel contains both amplitude and phase information of the radar signal, and the phase difference, obtained by multiplying the Master image with the complex conjugate of the Slave image, produced the interferogram. The resulting fringe patterns represent a combination of vertical and horizontal displacements, atmospheric effects, and noise. Simultaneously, a coherence map was generated for each image pair, indicating the signal stability and quality on a scale from 0 to 1; values close to 1 represent high stability (e.g., urban areas or unchanged surfaces), while values near 0 indicate low stability (e.g., dense vegetation or rapidly changing surfaces). This coherence map was used to assess interferogram quality and select reliable areas for subsidence analysis (Manzoni et al., 2021). To reduce the inherent speckle noise in SLC data, the Goldstein filter was applied, which enhances the main phase patterns and suppresses random noise through local-frequency analysis of the interferogram (Shukla et al., 2023). The phase is stored as wrapped phase, and to obtain a continuous map of actual ground deformation, phase unwrapping was performed using the

SNAPHU algorithm. To correct the data and align it with reference maps, the interferograms were projected to the WGS84 coordinate system, and topographic components were removed using the 30 m SRTM Digital Elevation Model (DEM). Atmospheric effects were corrected using GACOS data, and when these corrections were insufficient, time-series smoothing was applied with the MintPy library to retain only the true ground displacement.

1.2.2 SBAS

To extract ground subsidence, the Small Baseline Subset (SBAS) method was employed, which enables the measurement of gradual ground displacements with millimeter-level precision. In this approach, image pairs with small temporal and spatial baselines are selected to minimize the effects of surface cover changes and atmospheric conditions, producing a coherent network of ground deformation time series. The input data included unwrapped phase interferograms and coherence maps. Coherence maps were smoothed using a uniform filter, and low-coherence pixels were removed to ensure that only reliable data were used in SBAS calculations. Additionally, unwanted phase jumps were identified and corrected. Subsequently, the SBAS design matrix was constructed to define the temporal span of each interferogram, and a weight matrix (W) based on coherence was applied so that higher-quality data would have greater influence in the computations. To reduce temporal fluctuations, a smoothing constraint matrix (L) was applied. The SBAS equation was solved considering matrices A, W, L, and a numerical regularization term (λI) to stabilize the calculations (Zhaoying et al., 2016; Samsonov, 2019). Displacement along the satellite line of sight (LOS) was then calculated and converted to true vertical ground displacement using the satellite's viewing angle.

$$1)\ Vertical\ displacement = \frac{LOS}{COS^{\theta}}$$

1.2.3 Accuracy assessment

In this study the satellite viewing angle was set to 39 degrees based on Sentinel-1 metadata. To ensure the accuracy of InSAR processing and subsidence rate extraction, several key metrics were calculated. The coefficient of determination (R^2) was used for each pixel to assess the fit of displacement data to the trend line, the standard error of the slope evaluated confidence in the trend slope, and the annual mean coherence assessed data quality and temporal changes. A valid mask was also created to use only pixels with reliable observations, and the number of annual observations was normalized between 0 and 1, enabling robust subsidence analysis and reducing noise effects.To evaluate the accuracy of the SBAS algorithm, synthetic data were simulated. A 50×50 pixel grid with a subsidence rate of 10 millimeters per year and 61 imaging dates was generated. Interferograms were calculated for time intervals of 6, 12, and 24 days, and synthetic phase was produced by adding random noise and ±π phase jumps to mimic real data. Coherence values were randomly assigned between 0 and 1 to match the structure of Sentinel-1 data. The data were saved as GeoTIFFs and all SBAS processing steps were applied. Algorithm accuracy was evaluated using mean absolute error (MAE), root mean square error (RMS), and the coefficient of determination (R^2). Low MAE and RMS values indicated close agreement between simulated and real data with low error dispersion, while R^2 values confirmed a high match between retrieved results and true values, validating the SBAS algorithm under controlled conditions.

1.2.4 Classification and calculation of parameters

In this study, Pearson's correlation coefficient was used to examine the relationship between land subsidence and agriculture. The Pearson coefficient is a statistical measure that indicates the strength and direction of a linear relationship between two quantitative variables, ranging from -1 to +1. Values close to +1 indicate a strong positive correlation, values near -1 indicate a strong negative correlation, and values around zero suggest no correlation (Pearson., 1985).
To classify agricultural lands, Landsat satellite images with a spatial resolution of 30 meters for the years 2015 and 2023 were used. The classification was performed using the Random Forest algorithm, which relies on an ensemble of decision trees and combines their outputs to provide robust performance against noise and high accuracy in distinguishing land-use classes. For model training, 1,000 training samples were selected using stratified sampling to ensure balanced representation of all land-use classes. Classification accuracy was evaluated using 600 independent validation points through a confusion matrix, overall accuracy, and the Kappa coefficient, ensuring the reliability and validity of the results. To investigate the factors influencing the distribution and intensity of land subsidence in agricultural areas, topographic data from the Shuttle Radar Topography Mission (SRTM) digital elevation model with a spatial resolution of 90 meters were used. These data were obtained from the USGS and employed to derive two primary variables, slope and aspect. Slope is one of the most important factors affecting surface runoff, water infiltration, and soil stability; low-slope areas generally act as zones of water and sediment accumulation and are more prone to subsidence, whereas steep areas, due to better drainage, exhibit greater stability (Huat et al., 2006; Sekkeravani et al., 2022). Aspect also influences solar radiation reception, temperature, and evaporation, thereby affecting soil moisture, plant growth, and groundwater extraction. Directions with higher moisture content typically support more stable vegetation and greater resistance to subsidence (Varga & Csiszér, 2021). Finally, slope was mapped in percent, and aspect was classified into eight main categories: north, northeast, east, southeast, south, southwest, west, and northwest. To assess vegetation and soil moisture indices, Landsat satellite images from 2015 and 2023 were used. These images, with a spatial resolution of 30 meters, were processed in the Google Earth Engine environment. The Normalized Difference Vegetation Index (NDVI) was calculated for all four seasons—spring, summer, autumn, and winter—to capture seasonal variations in vegetation cover throughout the year. Healthy vegetation indicates adequate water availability and soil stability, whereas a decrease in NDVI typically reflects drought, groundwater depletion, or soil structure degradation, all of which can contribute to land subsidence (Ouyang et al., 2024). Therefore, NDVI was used as an indirect biophysical indicator of subsidence intensity. This index was computed from the combination of the red (Red) and near-infrared (NIR) bands as follows:

$$2)\ NDVI = \frac{NIR - RED}{NIR + RED}$$

Soil moisture reduction is one of the primary indicators of excessive groundwater extraction and compaction of soil layers. Therefore, analyzing soil moisture variations helps to better understand the dynamic behavior of soil in response to subsidence (Guo & Martinez-Grana et al., 2024). The Soil Moisture Index (SMI) was calculated for the four seasons—spring, summer, autumn, and winter—based on the relationship between NDVI and Land Surface Temperature (LST) (Saha et

This contribution has been peer-reviewed. The double-blind peer-review was conducted on the basis of the full paper.
https://doi.org/10.5194/isprs-annals-X-4-W8-2025-257-2026 | © Author(s) 2026. CC BY 4.0 License.

al., 2019). LST for each pixel was derived using the thermal band of Landsat 8 images. To determine soil moisture, the maximum and minimum surface temperatures corresponding to each NDVI value were first identified. These values represent the temperature range of hot and cold points and were obtained through linear regression of LST against NDVI. The SMI was then computed by comparing the actual temperature of each pixel with this maximum and minimum range.

$$3)\ SMI = (LST_{max} - LST)(LST_{max} - LST_{min})$$

where LST is the land surface temperature of a pixel, and ***LSTmax*** and ***LSTmin*** are the maximum and minimum surface temperatures for a given NDVI value, respectively.

1.2.5 Calculation of Land Subsidence Risk in Agricultural Lands

To assess subsidence risk in Golestan Province, land subsidence maps for 2015 and 2023, derived from Sentinel-1 data using the SBAS method, were imported as raster matrices for analysis. To standardize the data and enable integration with other environmental and agricultural indices, subsidence values for each pixel were normalized to the range [0,1]. NDVI and SMI indices were prepared for the four seasons (winter, spring, summer, and autumn). Each index was standardized using min-max normalization to ensure all indices shared a common scale and could be directly integrated with the subsidence maps. The risk index for each pixel was then calculated by multiplying the normalized index values by the subsidence magnitude. In other words, for each season, subsidence risk at each pixel was determined based on both the intensity of subsidence and the environmental or agricultural conditions of that pixel. Seasonal values were subsequently aggregated to generate annual risk maps for 2015 and 2023, allowing the analysis of temporal changes in risk and the identification of areas with increasing or decreasing hazard. To assess the changes in subsidence risk in the agricultural lands of Golestan Province between 2015 and 2023, the risk values were divided into ten equal intervals (0–0.1, 0.1–0.2, …, 0.9–1.0), and the number of pixels in each interval was calculated. This approach allows for examining the density of areas with low, medium, and high risk, as well as enabling direct comparisons between years. By analyzing the histogram, the concentration of pixels within specific risk ranges, seasonal or annual variations, and the intensity of risk increase or decrease can be quantified and visualized. A density plot for the risk values of each year was also generated to illustrate the continuous spatial distribution of risk across the province. Unlike the histogram, this method captures smooth variations and highlights concentrated or dispersed patterns of high-risk areas without dependency on interval size. The mean and standard deviation of risk values were calculated for each year to provide an overview of the average risk and its variability across the province. These metrics serve as a basis for analyzing trends and the concentration of high-risk areas. To determine whether the increase in mean risk in 2023 compared to 2015 is statistically significant, a paired t-test was applied. In this test, each pixel's risk value was compared pairwise across the two years, ensuring that the observed increase in risk is not merely due to random variation.

3. Results

The accuracy assessment of data extracted from radar interferograms indicated that the results are highly reliable. The mean coefficient of determination (R^2) was 0.78, reflecting a strong correlation between the modeled data and observed values. Additionally, the mean standard error of the slope was calculated as 0.00054, demonstrating the stability and high accuracy of the regression estimates. Furthermore, the average coherence of the images was 0.91, confirming the quality of the phase information and the robustness of the interferometric processing. To further evaluate the accuracy of the SBAS model, synthetic data simulations were conducted. The results indicated that the model exhibits high efficiency and precision. The mean absolute error (MAE) was 2.3 mm, the root mean square error (RMS) was 2.1 mm, and the coefficient of determination (R^2) reached 0.98. These values demonstrate that the SBAS model was able to reconstruct land subsidence variations with minimal error and high accuracy, ensuring a high level of confidence in the results (Figure 2). For Golestan Province in 2015, the results showed that land subsidence ranged from 0.36 to 3.57 cm (Figure 2). Spatial distribution analysis revealed that the highest displacement values occurred in the western parts of the province, primarily consisting of agricultural plains under intense farming pressure. By 2023, the extent of subsidence-affected areas had significantly expanded, and the intensity of ground displacement increased throughout these regions (Figure 3). During this year, surface displacement ranged from 4.1 to 4.56 cm, with no areas exhibiting subsidence below 4 cm, indicating a substantial intensification of subsidence in susceptible regions. The concentration of subsidence remained predominantly in agricultural areas.

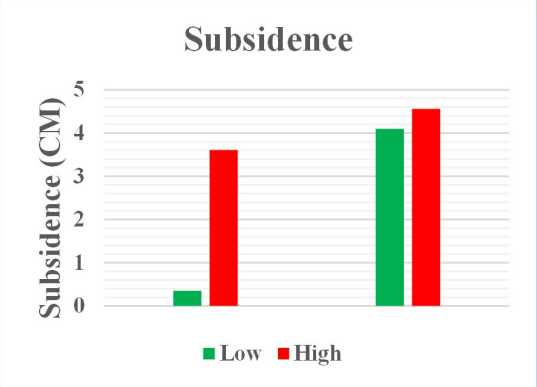

Figure 2. Comparative diagram of subsidence in 2015 and 2024

The accuracy of agricultural land classification for the years 2015 and 2023 was estimated at 87%. Moreover, correlation analysis between land subsidence and agricultural activity in Golestan Province revealed that agricultural land use exhibited a correlation of 0.71 with subsidence, indicating that agricultural practices play a significant role in land subsidence. Statistical analysis of land subsidence risk maps shows that considerable changes occurred in Golestan Province between 2015 and 2023 (Table 1). Comparative analysis of the subsidence risk maps indicated that 89% of pixels with a risk above 0.5 in 2015 also experienced subsidence in 2023. In 2015, the mean subsidence risk was calculated as 0.397 with a standard deviation of 0.110. This indicates that most areas under study were under moderate risk, with notable variability reflecting the presence of both low- and high-risk zones across the province. In other words, agricultural areas affected by subsidence were primarily in the moderate-risk range, and the intensity of land subsidence varied across different parts of the province. In 2023, the mean risk increased to 0.750, while the standard deviation decreased to 0.026. The rise in the mean indicates that land subsidence intensified across the entire province, whereas the reduction in

standard deviation reflects a more uniform risk pattern and greater convergence of high-risk areas. These changes suggest that nearly all agricultural areas in the province are now exposed to high risk, with low-risk zones almost entirely eliminated. Based on pixel-level data, a paired t-test was conducted to statistically evaluate risk changes between 2015 and 2023. The results showed a t-statistic of 3100.599 and a p-value ≈ 0, indicating a highly significant increase in risk. Therefore, it can be concluded that the observed changes are not random and that the intensity and extent of subsidence risk have genuinely increased. Analysis of pixel frequency across different risk intervals (0–1) also revealed substantial changes between 2015 and 2023. In 2015, most pixels fell within the 0.3–0.4 range (753,330 pixels), indicating that risk was concentrated at a moderate level. Very few pixels were in the >0.7 range, meaning high-risk areas were limited and scattered. By 2023, the highest pixel frequency had shifted to the 0.7–0.8 range (836,320 pixels), showing an upward shift in risk distribution, with large portions of the province now under high risk. Low-risk intervals were almost empty, reflecting a widespread increase in subsidence intensity. These distribution changes indicate that land subsidence has spatially expanded, affecting nearly all agricultural areas in the province rather than being confined to specific locations (Figure 4).

4. Discussion

This study investigated the spatial and temporal dynamics of subsidence risk in the agricultural lands of Golestan Province

Indicator	2015	2023	Statistical Test Indicators (2015–2023)
Mean subsidence risk	0.397	0.750	–
Standard deviation	0.110	0.026	–
Highest pixel frequency range	0.3–0.4	0.7–0.8	–
Paired t-test (t-statistic)	–	–	3100.599
Significance level (p-value)	–	–	≈ 0

Table 1. Statistical analysis of land subsidence risk and agricultural correlation in Golestan Province (2015–2023)

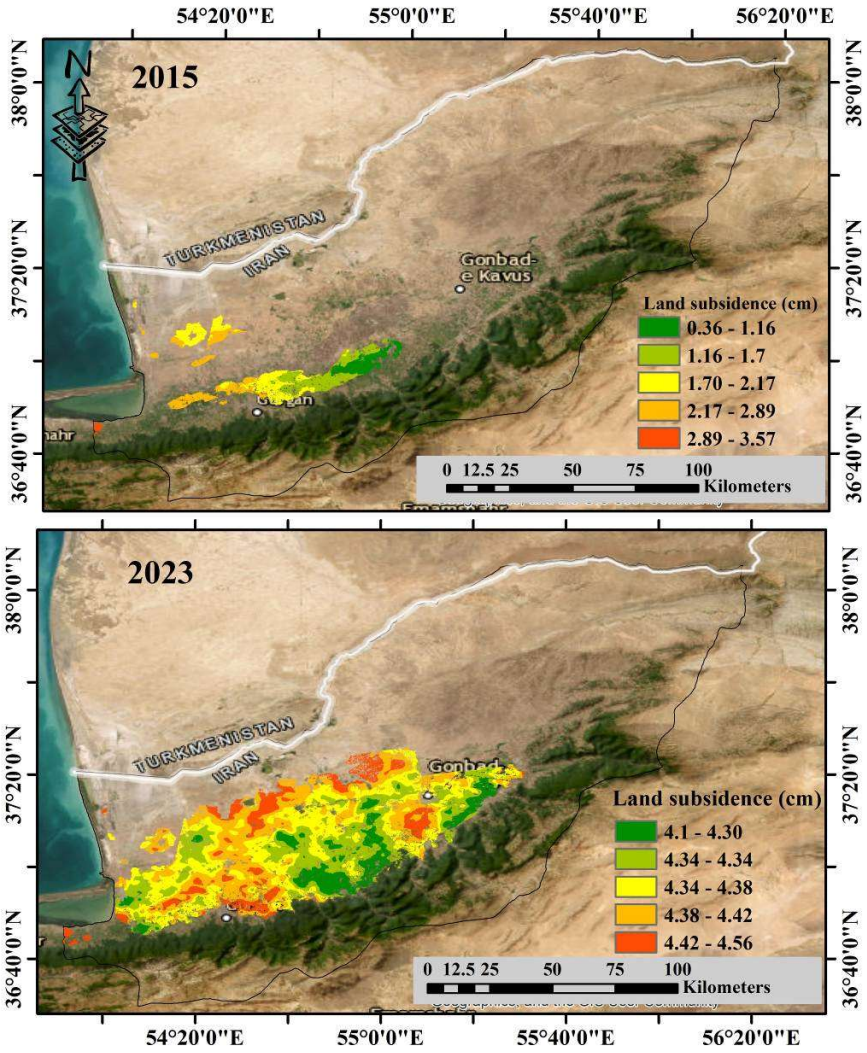

Figure 3. Subsidence map in agricultural lands for the years 2015 and 2023

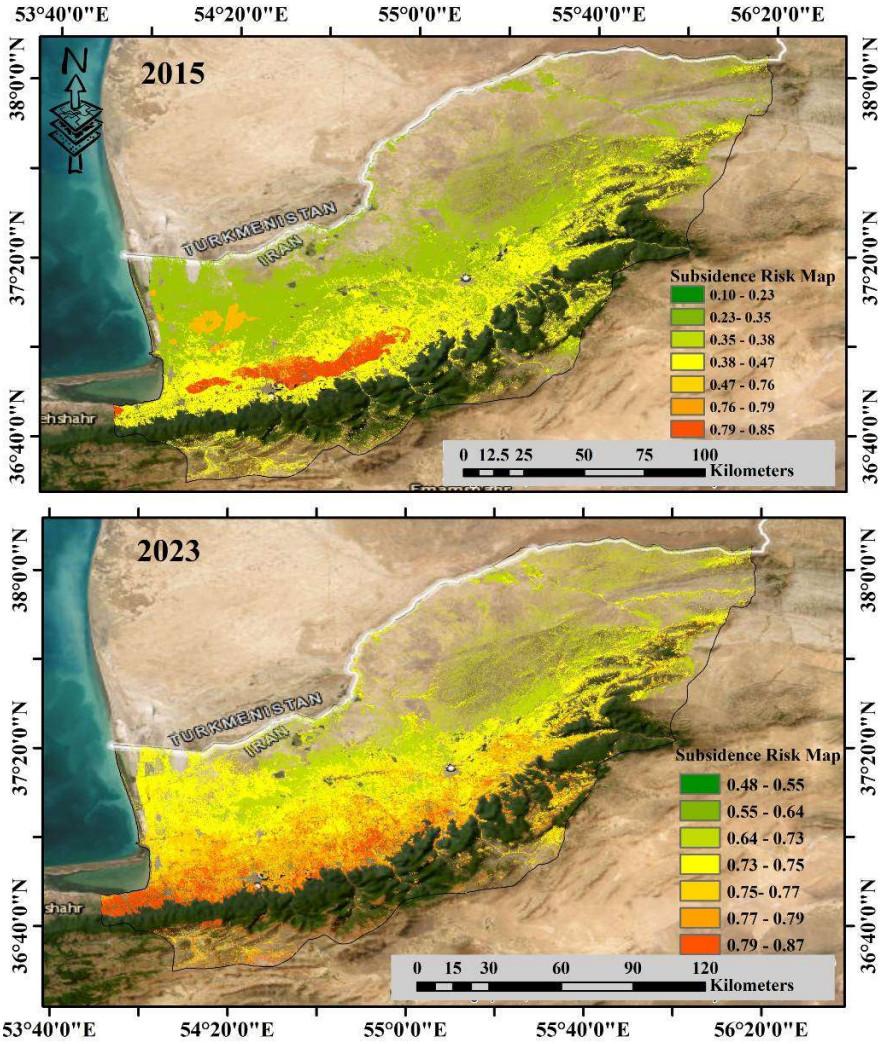

Figure 4. Risk map of land subsidence in agricultural lands for the years 2015 and 2023

between 2015 and 2023. Interferometric synthetic aperture radar (InSAR) data, combined with vegetation indices (NDVI), soil moisture (SMI), slope, and aspect, were used to examine environmental changes and their influence on subsidence. Unlike previous studies that primarily focused on average subsidence (Sidiq et al., 2019; Lechner et al., 2016), this research employs multi-seasonal data and environmental indicators to provide a more comprehensive perspective on subsidence risk in agricultural lands. The observed upward trend in mean subsidence risk—from 0.397 in 2015 to 0.750 in 2023—along with decreased variability, points to an increasing spatial uniformity of high-risk zones. Statistical results from paired t-tests ($t = 3100.599$, $p \approx 0$) reinforce that these patterns are systematic rather than random variations. The spatial correspondence between areas identified as high-risk in 2015 and those showing measurable deformation in 2023 indicates that regions under intensive agricultural use remain particularly susceptible to ground displacement. Similarly, reductions in NDVI and SMI values appear to coincide with regions of greater deformation, suggesting that changes in vegetation cover and soil moisture conditions may influence the observed subsidence patterns. These findings are consistent with those reported by Xiao et al. (2021) and Assadi et al. (2024), who also emphasized the influence of environmental stressors on subsidence dynamics. Integrating indices with InSAR data provides a robust framework for risk assessment. Therefore, this integrative approach not only strengthens the interpretation of subsidence mechanisms but also provides a transferable analytical framework that can inform sustainable land-use and agricultural water management strategies in similar vulnerable regions.

5. Conclusion

The primary objective of this study was to examine the changes in subsidence risk in agricultural lands of Golestan Province between 2015 and 2023 and to analyze the influence of environmental indicators (vegetation cover and soil moisture) on this phenomenon. The results demonstrated that the use of multi-seasonal NDVI, SMI, slope, and aspect data enables more accurate identification of agricultural lands at high risk of subsidence and provides a precise representation of the spatial variations and intensity of subsidence. The increase in mean risk and the homogenization of high-risk areas between 2015 and 2023 indicate an intensification of subsidence and underscore the importance of sustainable management of agricultural resources and food security. Based on these findings, it can be concluded that integrating environmental indicators with InSAR data offers

an effective framework for assessing subsidence risk in agricultural lands and provides practical insights for agricultural planning and land management. For future research, it is recommended to utilize higher spatial resolution remote sensing data to more accurately evaluate the impact of agricultural practices and land use patterns on subsidence risk, extend the study period to analyze long-term trends and the effects of climate change on agricultural areas and subsidence, and develop integrated regression or machine learning models for more precise prediction of subsidence-prone areas in relation to agricultural activities and environmental indicators.

References

Assadi, M. A. Z., Nasiri, A., Zandi, R., Shafiei, N., 2024. Impact of crop types on land subsidence: a case study of Nourabad aquifer, Iran. Environmental Monitoring and Assessment, 196(12), 1271. https://doi.org/10.1007/s10661-024-13453-w

Ashournejad, Q., Garshasbi, F., 2024. Economic valuation of changes in ecosystem services of 77 Ramsar wetlands in West Asia over 37 years (1984–2021). Environmental Conservation, 51(3), 196-202. https://doi.org/10.1017/S0376892924000183

Rufai, A. A., Doma, I. M., 2024. Assessment of Land Use Changes Using Remote Sensing and Geographic Information System (GIS) in Kumbotso Local Government Area, Kano State. *International Journal of Research Publication and Reviews*. https://doi.org/10.55248/GENGPI.5.0624.1635

Merem, E. C., Twumasi, Y., Wesley, J., Alsarari, M., Fageir, S., Crisler, M., Washington, J., 2019. Analyzing land use and change detection in Eastern Nigeria using GIS and remote sensing. *American Journal of Geographic Information System*, *8*(2), 103-117. https://doi.org/10.5923/j.ajgis.20190802.06

Guo, H., Martinez-Grana, A. M., 2024. Correlation between Soil Moisture Change and Geological Disasters in E'bian Area (Sichuan, China). *Applied Sciences*, *14*(15), 6685. https://doi.org/10.3390/app14156685

Huat, B. B., Ali, F. H., Low, T. H., 2006. Water infiltration characteristics of unsaturated soil slope and its effect on suction and stability. *Geotechnical & Geological Engineering*, *24*(5), 1293-1306. https://doi.org/10.1007/s10706-005-1881-8

Lechner, A. M., Baumgartl, T., Matthew, P., Glenn, V., 2016. The impact of underground longwall mining on prime agricultural land: a review and research agenda. *Land Degradation & Development*, *27*(6), 1650-1663. https://doi.org/10.1002/ldr.2303

Manzoni, M., Molinari, M. E., Monti-Guarnieri, A., 2021. Multitemporal InSAR coherence analysis and methods for sand mitigation. *Remote Sensing*, *13*(7), 1362. https://doi.org/10.3390/rs13071362

Manzoni, M., Molinari, M. E., Monti-Guarnieri, A., 2021. Multitemporal InSAR coherence analysis and methods for sand mitigation. *Remote Sensing*, *13*(7), 1362. https://doi.org/10.3390/rs13071362

Ouyang, L., Zhao, Z., Zhou, D., Cao, J., Qin, J., Cao, Y., He, Y., 2024. Study on the relationship between groundwater and land subsidence in Bangladesh Combining GRACE and InSAR. *Remote Sensing*, *16*(19), 3715. https://doi.org/10.3390/rs16193715

Pearson, K., 1895. VII. Note on regression and inheritance in the case of two parents. *proceedings of the royal society of London*, *58*(347-352), 240-242. https://doi.org/10.1098/rspl.1895.0041

Saha, A., Patil, M., Goyal, V. C., Rathore, D. S., 2019. *Assessment and impact of soil moisture index in agricultural drought estimation using remote sensing and GIS techniques. Proceedings 7: 2*. https://doi.org/10.3390/ECWS-3-05802

Samsonov, S., 2019. Three-dimensional deformation time series of glacier motion from multiple-aperture DInSAR observation. *Journal of Geodesy*, *93*(12). https://doi.org/10.1007/s00190-019-01325-y

Sekkeravani, M. A., Bazrafshan, O., Pourghasemi, H. R., Holisaz, A., 2022. Spatial modeling of land subsidence using machine learning models and statistical methods. *Environmental Science and Pollution Research*, *29*(19), 28866-28883. https://doi.org/10.1007/s11356-021-18037-6

Sidiq, T. P., Gumilar, I., Abidin, H. Z., Gamal, M., 2019. Land subsidence induced by agriculture activity in Bandung, West Java Indonesia. In *IOP Conference Series: Earth and Environmental Science* 389(1), p. 012024. IOP Publishing. https://doi.org/10.1088/1755-1315/389/1/012024

Ashraf, T., Yin, F., Liu, L., Zhang, Q., 2024. Land Subsidence Detection Using SBAS-and Stacking-InSAR with Zonal Statistics and Topographic Correlations in Lakhra Coal Mines, Pakistan. *Remote Sensing*, *16*(20), 3815. https://doi.org/10.3390/rs16203815

Sun, T., Cheng, W., Abdelkareem, M., Al-Arifi, N., 2022. Mapping prospective areas of water resources and monitoring land use/land cover changes in an arid region using remote sensing and GIS techniques. *Water*, *14*(15), 2435. https://doi.org/10.3390/w14152435

Varga, C., Csiszér, L., 2020. The influence of slope aspect on soil moisture. *Acta Univ. Sapientiae Agric. Environ*, *12*, 82-93. https://doi.org/10.2478/ausae-2020-0007

Xiao, W., Zheng, W., Zhao, Y., Chen, J., Hu, Z., 2021. Examining the relationship between coal mining subsidence and crop failure in plains with a high underground water table. Journal of Soils and Sediments, 21(8), 2908-2921. https://doi.org/10.1007/s11368-021-02991-2

Zhaoying, J. I. A. N. G., Guolin, L. I. U., Qiuxiang, T. A. O., 2016. Regularization solution of small baseline subset deformation model inversion. Acta Geodaetica et Cartographica Sinica, 45(5), 566. https://doi.org/10.11947/j.AGCS.2016.20150143